

## Vertically self-organized Ge/Si(001) quantum dots in multilayer structures

Vinh Le Thanh,\* V. Yam, and P. Boucaud

*Institut d'Électronique Fondamentale, UMR-CNRS 8622, Bâtiment 220, Université Paris-Sud, 91405 Orsay Cedex, France*

F. Fortuna

*Centre de Spectrométrie Nucléaire et de Spectrométrie de Masse, IN2P3-CNRS, Bâtiment 108, Université Paris-Sud, 91405 Orsay Cedex, France*

C. Ulysse, D. Bouchier, L. Vervoort, and J.-M. Lourtioz

*Institut d'Électronique Fondamentale, UMR-CNRS 8622, Bâtiment 220, Université Paris-Sud, 91405 Orsay Cedex, France*

(Received 25 January 1999; revised manuscript received 28 April 1999)

*In situ* reflection high-energy electron diffraction along with transmission electron microscopy, atomic force microscopy, and photoluminescence spectroscopy have been used to investigate the Ge growth behavior in a standard Ge/Si multilayer structure. It is shown that the decrease of the Ge wetting layer thicknesses in the upper layers of a multilayer structure is the main parameter which leads to the increase of the island size and height. Such an evolution of the Ge wetting layer thickness can be explained by an accumulation of elastic strain in the Si spacer layers induced by the lower Ge wetting layers. This finding opens the route to the realization of a multilayer structure in which the islands have equal size in all layers. [S0163-1829(99)03132-X]

During the last few years, much effort has been devoted to creating Ge/Si quantum dots (QD's), as these structures are expected to be potential candidates for the realization of silicon-based quantum electronic and optoelectronic devices.<sup>1</sup> In particular, it has been recently demonstrated that the Ge/Si(001) QD's exhibit intraband absorption at  $\sim 300$  meV, thus opening the route towards the fabrication of mid-infrared QD-based photodetectors.<sup>2</sup> Among the different ways to produce QD's, the self-assembled technique, which takes advantage of the strain-driven transition from two-dimensional (2D) to three-dimensional (3D) growth mode (Stranski-Krastanow growth),<sup>3</sup> has received particular interest since this technique could allow one to produce quantum sized islands without needing any kind of mask or patterning. However, due to the random process of islanding nucleation, the self-assembled technique suffers from broad distributions both in size and in position. Although in a recent work we have presented the ways to obtain uniform island in a single layer,<sup>4</sup> but their formation has been found to depend critically on the growth parameters, such as the deposited coverage and the growth temperature.

Recently, it has been shown that starting from a single layer with inhomogeneous islands one can finally obtain uniform islands by growing multilayer structures, i.e., structures which consist of successive layers of pure Ge (or of SiGe alloys) separated by Si barrier layers.<sup>5,6</sup> An interesting feature observed in multilayer structures is that the islands in the upper layers grow on the top of the buried ones, giving rise to a vertical correlation between islands along the growth direction. This vertical self-organization has been observed both in InAs/GaAs (Refs. 7 and 8) and Ge/Si (Refs. 5, 6 and 9–13) systems, while its origin has been attributed, for instance, to preferential nucleation<sup>5</sup> or directional adatom migration<sup>7</sup> due to inhomogeneous strain fields induced by buried islands. Another general trend observed in multilayer

structures is that the average island base size increases with increasing the number of deposited layers (an increase by a factor of about 3 has been, for example, obtained in Refs. 5 and 6 after the deposition of 20 SiGe/Si bilayers). The increase in the island size has not received up to now a clear explanation, but from the technological point of view this may be considered as one of the main drawbacks for the application of multilayer arrays. Indeed, for most QD-based applications it is desirable to have islands with sizes as small as possible to obtain an efficient quantum confinement inside the islands. In a recent paper, Mateeva *et al.*<sup>12</sup> have proposed, on the basis of TEM investigations, that the merging of small islands is the main mechanism leading to the increase of the island size and the improvement of their size uniformity. This proposal, in our opinion, can not be generalized for at least two reasons. First, the authors treat a case in which the vertical correlation between islands occurred only after the deposition of a certain number of layers ( $\sim 10$ – $15$  layers). This is not the general case of multilayer structures.<sup>7,10,11</sup> Secondly, according to the merging mechanism, the island size should be stabilized when the vertical correlation is achieved. This is not coherent with previous results [see, for example, Fig. 1(c) of Ref. 7, and Refs. 10, 11, and 13], in which the average island size still increased after the one-to-one vertical correlation had been achieved. We also note that in *all* previous works the authors have mainly focused on the influence of the thickness of the barrier layers<sup>6,7</sup> or the growth parameters (growth temperature, growth rate<sup>10,11</sup>) on the self-organization, but very little attention has been paid to the growth mode of Ge (or InAs) itself.

In this work, we investigate the Ge growth behavior in a Ge/Si(100) multilayer structure. To understand the growth in the most general manner as possible, we have considered a *standard* self-organized system, a system that exhibits a high

vertical correlation. The advantage of our work consists of the use of *in situ* reflection high-energy electron diffraction (RHEED) to precisely monitor in real time the Ge 2D-3D growth mode transition. To further elucidate the RHEED analysis, post-growth investigations have been performed in combining optical and structural characterizations.

Experiments were carried out in an ultrahigh-vacuum chemical-vapor deposition (UHV-CVD) system. Pure SiH<sub>4</sub> and hydrogen-diluted (10%) GeH<sub>4</sub> were used as gas sources. The system has a base pressure better than  $1 \times 10^{-10}$  Torr, and the pressure during growth was about  $5 \times 10^{-4}$  Torr. The growth chamber is equipped with a differentially pumped RHEED system, allowing us to probe the growing surface even at high partial pressures of hydrides (up to  $10^{-1}$  Torr). During experiments, RHEED patterns were recorded using a camera-based video recording system. Details of the experimental setup and growth conditions have been reported elsewhere.<sup>14</sup> Photoluminescence (PL) measurements were performed at low temperatures, using an Ar<sup>+</sup> laser (power density of 400 mW/cm<sup>2</sup>). The PL signal was detected with a liquid-nitrogen-cooled Ge photodetector using a standard lock-in technique. Atomic force microscopy (AFM) images were recorded with a Park Scientific Instruments AFM setup operating in contact mode. Transmission electron microscopy (TEM) measurements were performed on cross sections using a 400 kV microscope.

The Ge growth temperature was chosen to be 550 °C, based on our recent work which established that growing at this temperature results in a relatively narrow size distribution of islands.<sup>4</sup> The Ge growth rate determined from the RHEED oscillations was 1 monolayer (ML) per minute (1 ML = 1.457 Å). Due to a very low Si growth rate at 550 °C, Si deposition was carried out at 600 °C and without growth interruption to avoid island coalescence (Si deposition was started at 550 °C, the growth temperature was then slowly raised to 600 °C). The Si growth rate determined from high-resolution TEM was of 2.2 nm/min. The thickness of the Si spacer layers was chosen to be ~22 nm, not too thick in order to preserve a high vertical correlation between islands, but also not too thin in order to avoid interactions between islands in different layers which may result in the formation of cone-shaped defects.<sup>9</sup> Two main series of samples were grown. The first, serving as reference samples, consists of a single Ge layer, covered or not with a Si cap layer for PL and AFM investigations, respectively. The second series consists of 10 Ge/Si periods, the last Ge layer being not covered with Si for AFM analysis.

Figure 1 shows a representative [011] cross-sectional TEM image of a sample with 10 Ge/Si bilayers. Regions of dark contrast correspond to the thin Ge wetting layers (WL's) and Ge islands, while light contrast regions correspond to the Si spacer layers. The amount of deposited Ge in each layer was chosen to be equal to the critical thickness determined for the first layer (this thickness has been considered as the thickness at which the transition from 2D to 3D growth mode occurred). The critical thickness determined from RHEED oscillations was of 4 ML's, the corresponding growth time ( $t_g$ ) was 240 s. The Ge amount was kept constant during the deposition of the upper layers. The image clearly shows that each island in the upper layers grows on the top of the islands in the lower layers, indicating a high

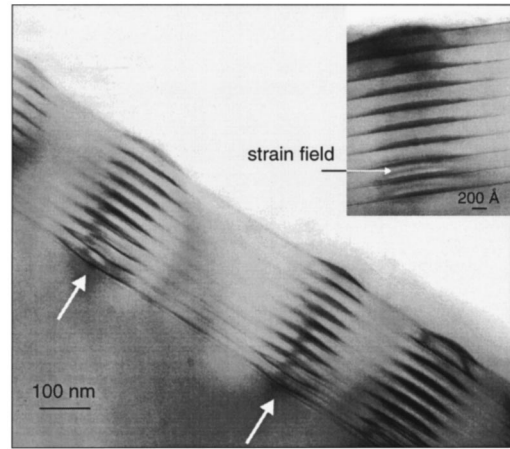


FIG. 1. Typical bright-field cross-sectional TEM image taken along the [011] azimuth of a sample with 10 Ge/Si bilayers. The deposited Ge amount was kept constant in all layers, the last Ge layer was not covered with Si. The image clearly shows that the islands on the upper layers grow on the top of the islands in the lower layers, giving rise to a high vertical correlation between islands. Shown in the inset is a zoom of an island column along the growth direction. The small arrow indicates the strain field induced in the Si spacer layers by buried islands.

vertical correlation between islands. It is worth noting that the vertical ordering already occurs for the second deposited layer, which is similar to what has been previously reported for both III-V (Ref. 7) and IV-IV heterostructures.<sup>8,10,11,13</sup> This indicates that the structure investigated here can be considered as a standard case of self-organization. Displayed in the inset of Fig. 1 is a zoom of an island column along the growth direction. Two main features can be clearly seen from this figure. First, the Si spacer layer appears to be thick enough to flatten the growth front prior to the deposition of each new Ge layer. Secondly but more importantly, the figure shows that the islands undergo a drastic change both in size and height from the first to the third layer, while they become almost stable from the fifth layer. It is interesting to note that the strain fields (indicated by a small arrow) induced by buried islands in the Si spacer layers are only observed in the first and second spacer layers. Figure 2 summarizes the evolution of the island size (left axis) and height (right axis) as a function of the number of deposited layers. The data have been obtained by evaluating about 20 island columns from [011] cross-sectional TEM images. The average island size is found to increase from ~100 nm in the first layer up to ~180 nm in the fifth layer and then remains nearly unchanged. Similar behavior is observed for the island height, which increases from ~8.6 nm in the first layer to ~12.3 nm in the fifth layer and becomes stable from the fifth layer on.

The increase of the island size and height is also confirmed from AFM measurements, as indicated in Fig. 3. We note that the island sizes measured from AFM are relatively in good agreement with those obtained from TEM while island heights are significantly overestimated. The overestimation of the island heights can be explained due to the convolution of the AFM tip with the islands, both having a comparable radius. However, since we are essentially interested in the variation of the island dimensions, the relative

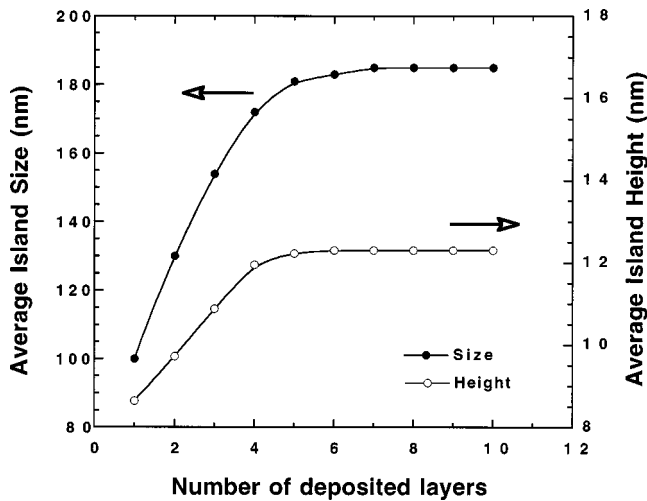


FIG. 2. Evolution of the island sizes (left axis) and island heights (right axis) as a function of the number of deposited layers. The data are obtained by evaluating about 20 island columns in cross-sectional TEM images. Full curves are only guides for the eye.

character of these values is not embarrassing. Figures 3(a) and 3(b) show an AFM image and a height profile along an island of an uncapped single-layer surface. It is important to note that the Ge growth was stopped just after the appearance of three-dimensional spots in the RHEED pattern, i.e., at the early stage of island nucleation. The corresponding Ge coverage was 4 ML's ( $t_g = 240$  s). The surface exhibits islands which are relatively uniform in size (a deviation of about 10%), but *randomly* distributed along the surface. The average size of islands is  $\sim 100$  nm, their height is about  $\sim 14$ – $15$  nm. The areal density of islands is  $\sim 1.3 \times 10^9 \text{ cm}^{-2}$ . The surface of an uncapped 10-bilayer sample is shown in Figs. 3(c) and 3(d). As can be seen in these figures, the islands have now a size of  $\sim 170$  nm and a height of  $\sim 21$  nm, these

two values being 1.4–1.5 times larger than those corresponding to the single layer. The island density is about  $2 \times 10^9 \text{ cm}^{-2}$ , that is slightly higher than that on the single layer. This indicates that there does not exist a real one-to-one island vertical correlation throughout the layers. It is interesting to note that the islands are now much more regularly distributed over the surface, thus indicating the benefit of lateral ordering in the multilayer structure. We note that very little is gained on the island size distribution as under the growth conditions investigated, in particular at a growth temperature of  $550^\circ\text{C}$ , the single-layer islands already exhibit a low dispersion in size.<sup>4</sup>

The photoluminescence spectrum of the same sample is shown in Fig. 4(b). For comparison, we report in Fig. 4(a) the PL spectrum of a single layer. The single layer was covered with a 22-nm thick Si cap layer, i.e., *identical* to the first bilayer of the multilayer sample. Apart from the narrow peak at 1098 meV which is attributed to the phonon-assisted recombination of the free-exciton in the Si substrate, the single-layer spectrum consists of two separate components characteristic of the Ge wetting layer WL and Ge islands, respectively. The WL component is characterized by two main lines located at  $\sim 1024$  and  $\sim 967$  meV, which are, respectively, due to the excitonic no-phonon (NP) and transverse-optical (TO)-phonon-assisted transitions of pseudomorphic Ge layers in Si.<sup>15</sup> The energy difference between the NP and TO lines is  $\sim 57$ – $58$  meV, which corresponds to the Si-Si optical phonon energy in Si.<sup>15</sup> The emission band lying at the lower energy, of  $\sim 768$  meV, is attributed to three-dimensional Ge islands as previously reported.<sup>4</sup> The multilayer spectrum also consists of two components as discussed above, but, importantly, both of them now contain two separate parts. The first part originates from the first layer while the second part can be attributed to the rest of the layers. The Ge WL component now contains four main lines, denoted  $\text{NP}_1$ ,  $\text{TO}_1$ ,  $\text{NP}_n$  and  $\text{TO}_n$ , instead of the

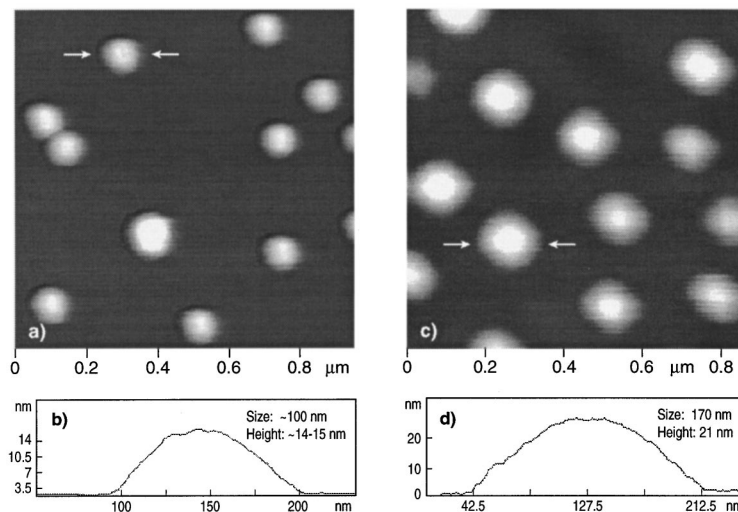


FIG. 3. Comparison of the surface morphology between single-layer and ten-bilayer samples. (a) and (b) correspond to the single-layer sample, (c) and (d) are for the multilayer sample. (a)  $0.95 \mu\text{m} \times 0.95 \mu\text{m}$  AFM image of a single-layer sample. Note that the Ge growth was stopped just after the appearance of three-dimensional spots in RHEED patterns, i.e., at the first stage of the island nucleation. The corresponding Ge coverage was 4 ML's. (b) AFM height profile along the island indicated by two small arrows in (a). (c)  $0.85 \mu\text{m} \times 0.85 \mu\text{m}$  AFM image of a ten-bilayer sample. Note that the deposited Ge amount was kept constant in all layers. (d) AFM height profile along the island indicated by two small arrows in (c).

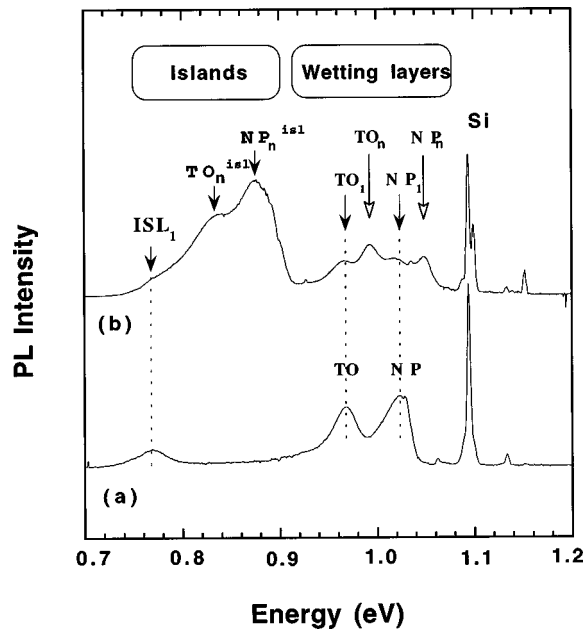


FIG. 4. 6 K photoluminescence spectra of a single layer (a) and of a ten-bilayer sample (b). The single layer is covered with a 22-nm thick Si cap layer, i.e., identical to the first bilayer in the multilayer sample. Note that the wetting layer and island components of the multilayer-sample spectrum consist of two separate subcomponents: the low-energy subcomponent ( $ISL_1, TO_1, NP_1$ ) originates from the first layer, while the subcomponent at higher energy side ( $TO_n^{isl}, NP_n^{isl}, TO_n$ , and  $NP_n$ ) can be attributed to the upper layers.

two ones observed in the single-layer spectrum. The  $NP_1$  and  $TO_1$  lines, which are located at the same energies as the NP and TO lines in the single-layer spectrum, can be unambiguously assigned to the no-phonon transition and its TO replica for the first Ge wetting layer. Two additional lines,  $NP_n$  and  $TO_n$ , are observed at higher energies of  $\sim 1048$  and  $\sim 991$  meV, respectively. Interestingly, the separation in energy between these two lines is still of  $\sim 57$ – $58$  meV, a value expected for the energy separation between the NP and TO lines of a pseudomorphic 2D Ge layer. The appearance of these two lines can then be interpreted as arising from other Ge wetting layers, which have a thickness smaller than that of the first layer. For the island-related component, three peaks, denoted to as  $ISL_1$ ,  $TO_n^{isl}$ , and  $NP_n^{isl}$ , can be resolved after a deconvolution by using a set of three gaussian line-shaped peaks, which have their maxima at 768, 833, and 875 meV, respectively. The fact that the energy position of the  $ISL_1$  peak is the same as that of the island-related peak in the single layer unambiguously indicates that this peak stems from the islands in the first layer. The other two peaks,  $NP_n^{isl}$  and  $TO_n^{isl}$  can be attributed to no-phonon and phonon-assisted transitions of islands from the second to the ninth layers. We assume that the uncapped last layer has no contribution to the PL due to nonradiative surface recombination. The energy separation between the  $NP_n^{isl}$  and  $TO_n^{isl}$  peaks is  $\sim 42$  meV, a value close to the  $TO_{Ge-Ge}$  phonon energy.<sup>15</sup> The separation of the island-related emission into two peaks NP and TO (or the appearance of a phonon-assisted transition), may be indicative of a decrease of the carrier localization inside the islands due to the increase of their sizes and

heights in the upper layers. On the other hand, the shift to higher energies of these two peaks compared to the  $ISL_1$  peak is presently not well understood. An almost similar effect has been observed in a five-bilayer Ge/Si structure.<sup>13</sup> It is worth noting that the islands in the first layer are nucleated on a Si surface that is strain free, while those in upper layers are nucleated on inhomogeneously strained Si surfaces. This implies that the strain state around and also inside the islands in the first layer is quite different from that of the islands in upper layers. The blue shift of the island-related peaks in the upper layers may arise from material interdiffusion assisted by strain fields and/or a variation of the strain state in the Si spacer layers and inside the island in the upper layers. We note that the effect of *thermal* interdiffusion between Si and Ge can be ruled out. As we have mentioned above, the Ge growth temperature was chosen to be 550 °C since at this temperature the islands exhibit a narrow size distribution.<sup>4</sup> Due to a very low Si growth rate at 550 °C, Si deposition was carried out at 600 °C. Even though care has been taken to minimize the Ge/Si interdiffusion (Si deposition was started at 550 °C, the growth temperature was then slowly raised to 600 °C), thermal interdiffusion between Ge and Si might occur at both interfaces during this increase of the growth temperature, which may result in a lower Ge content inside the islands, and therefore a blueshift of island-related peaks. However, since the growth temperatures for Ge and Si were the the same for the single-layer and multilayer samples, the effect of thermal interdiffusion was expected to be the same in both cases.

To further clarify the existence of other types of Ge WL's in the upper layers of the multilayer sample, we have undertaken a RHEED analysis, by measuring the transition from a two-dimensional to a three-dimensional growth mode during the Ge deposition in different layers of a ten-period sample. Since the transition to a 3D growth mode is characterized by the appearance of bulk-type diffraction spots,<sup>16</sup> we have measured the variation of the RHEED intensity of one of these spots as a function of the deposition time  $I(t_g)$ . A typical result for the first and the second layers of the ten-period sample is reported in Fig. 5(a). We note that the sample was grown in the same conditions as the one investigated in Figs. 1 and 4, i.e., each Ge layer was separated by a 22-nm thick Si spacer layer. Prior to the deposition of each new Ge layer, the Si surface exhibited a well-developed  $2 \times 1$  streaky RHEED pattern, indicating that the Si surface was smoothed out. The figure shows that the 2D-3D transition is very sudden, allowing a relatively precise determination of the corresponding critical thickness ( $h_c$ ). To precisely determine  $h_c$  in each layer, we searched the inflexion point  $M$  of  $I(t_g)$ , and assumed that  $h_c$  corresponds to the intersection point of the tangent at  $M$  with the base line. Shown in Fig. 5(b) is the evolution of the 2D-3D transition time and the critical thickness versus the total number of the deposited layers. The Ge critical thickness, which is of 4 ML's ( $t_g = 240$  s) for the first layer, is found to rapidly decrease within the three first layers and reaches a stable value of 2.08 ML's ( $t_g = 125$  s) after the fifth layer. As the result of RHEED analysis, the multilayer structure is found to present five critical thickness, which are of 4, 2.5, 2.25, 2.13, and 2.08 ML's for the first, second, third, fourth, and the last six layers, successively. The fact that only two WL-related

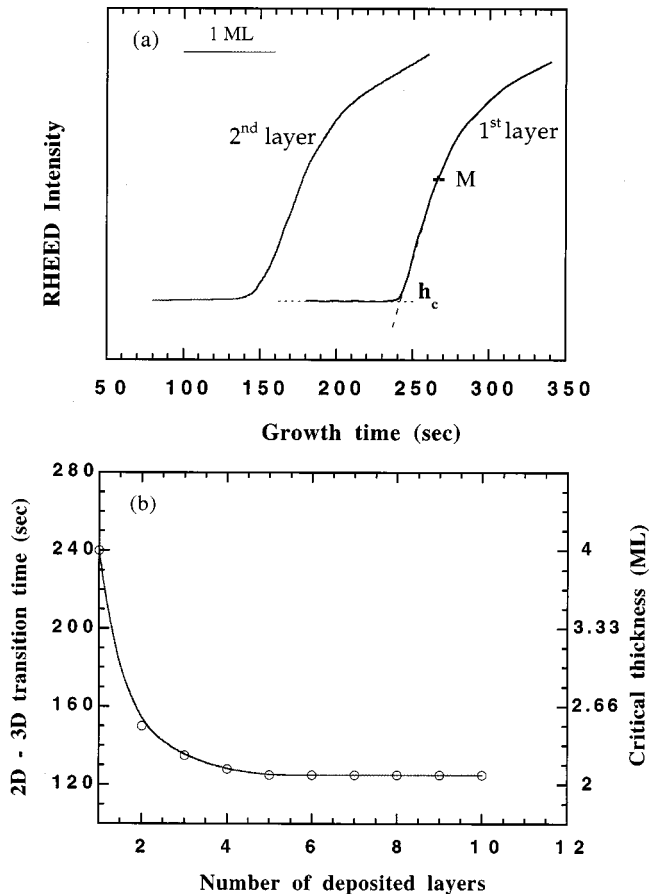


FIG. 5. (a) Intensity evolution of a bulk spot of the RHEED pattern as a function of the deposition time during the deposition of the first and second layers of a ten-period sample. Note that the growth time at which the transition from 2D to 3D growth mode occurs is observed at 150 s for the second layer compared to at 240 s for the first layer. The Ge growth rate is 1 ML/min. (b) Evolution of the 2D-3D transition time (to the left) and of the critical thickness (right axis) as a function of the number of deposited layers in a ten-period sample.

NP-TO pairs are observable in the corresponding PL spectrum [Fig. 4(b)] can be explained as follows. The pair at the lower energy side has been attributed to the first layer, the high-energy one might stem from the last six layers starting from the fifth one. The other layers in between have thicknesses very close to that of the last layers and may manifest themselves only in a broadening of the 2.08 ML-related PL lines. This assumption is supported by the fact that the energy position of the  $NP_n$  line, observed at 1048 meV, is very close to that of the NP line of a 2 ML-deposited sample ( $E_{NP} = 1039$  meV for  $t_g = 2$  min in Fig. 4 of Ref. 4). We finally note that the RHEED results provide a good explanation to the previously discussed results observed by TEM (Figs. 1 and 2). The increase of the island size and height from the second to the fifth layer and the stability of the island dimensions after the deposition of the fifth layer will correspond to the decrease of the Ge critical thickness observed by RHEED. The above structural and optical results have therefore indicated that the decrease of the Ge wetting layer thickness in the upper layers is responsible for the increase of the island size and height.

How can we explain such a behavior of the Ge wetting

layers? For the deposition of each new Ge layer, the growth process can be influenced by two parameters: the first one is the 4% compressive strain induced by the buried Ge wetting layer(s); the second one is the inhomogeneous strain field due to partially strain relaxed islands and the 4% compressively strained wetting layer in between them. The second parameter, which has been recognized to be responsible for the vertical ordering of islands,<sup>5-7</sup> is expected to play an important role only in the island nucleation process. To better see the influence of the first parameter on the observed decrease of the Ge wetting layers, we have grown a series of multilayer samples in which the thicknesses of the first Ge layer were chosen to be successively of 1, 2, and 3 ML's, while the Si spacer layer was kept constant (22 nm). As these thicknesses are smaller than the critical thickness (4 ML's) under the growth conditions investigated here, the misfit strain in the first layer can be considered to be homogeneous. Though the decrease rate of the Ge wetting layers is different depending on the Ge amount in the first layer, the Ge wetting layers behave in the same manner as that presented in Fig. 5(b). This indicates that the homogeneous strain field being induced by the buried Ge wetting layers and mediated by the Si spacer layers is the main parameter which leads to the decrease of the Ge WL thickness in the upper layers. At a given thickness of the first Ge layer, the thickness of the Si spacer layer was found to significantly influence the evolution of the Ge critical thickness and, as a consequence, the evolution of the island dimensions in subsequent layers. The number of layers at which the Ge critical thickness stabilizes may correspond to a saturation of accumulated elastic strain after the deposition of a certain number of layers. Of course, this layer number has not a fixed value, but was found to depend on the thickness of the initial Ge layer and that of the Si spacer layers. A detailed analysis of such an evolution as a function of the first layer Ge thickness and of the Si spacer layer thickness will be presented in a separate paper.

The finding of the decrease of the Ge 2D layer thickness in the upper layers of a multilayer structure has conducted us to a very simple idea for the realization of a multilayer structure in which the islands may have equal size in all layers. If one does not keep the Ge deposited amount constant in all layers (equal to the critical thickness of the first layer), but adjusts this amount according to the *effective* critical thicknesses in subsequent layers, this can lead to the formation of islands at the first nucleation stage in all layers. As a demonstration, a cross-sectional TEM image of an uncapped ten-bilayer sample produced with this method is shown in Fig. 6. A zoom of an island column along the growth direction is presented in Fig. 6(b). The Ge growth in *each* layer was stopped just after the appearance of three-dimensional spots in the RHEED pattern. The Si spacer-layer thickness was kept constant at 22 nm. As can be seen in Fig. 6(a), the islands still exhibit a high correlation along the growth direction. An important result is that the islands have now almost equal size and height in all layers [Fig. 6(b)], in contrast to the case presented in the inset of Fig. 1 in which the Ge amount was kept constant in all layers.

Figure 7 shows the surface morphology of the corresponding sample. As expected, the surface exhibits islands having dimensions much smaller than those obtained with a constant deposited Ge amount [Figs. 3(c) and 3(d)]. The av-

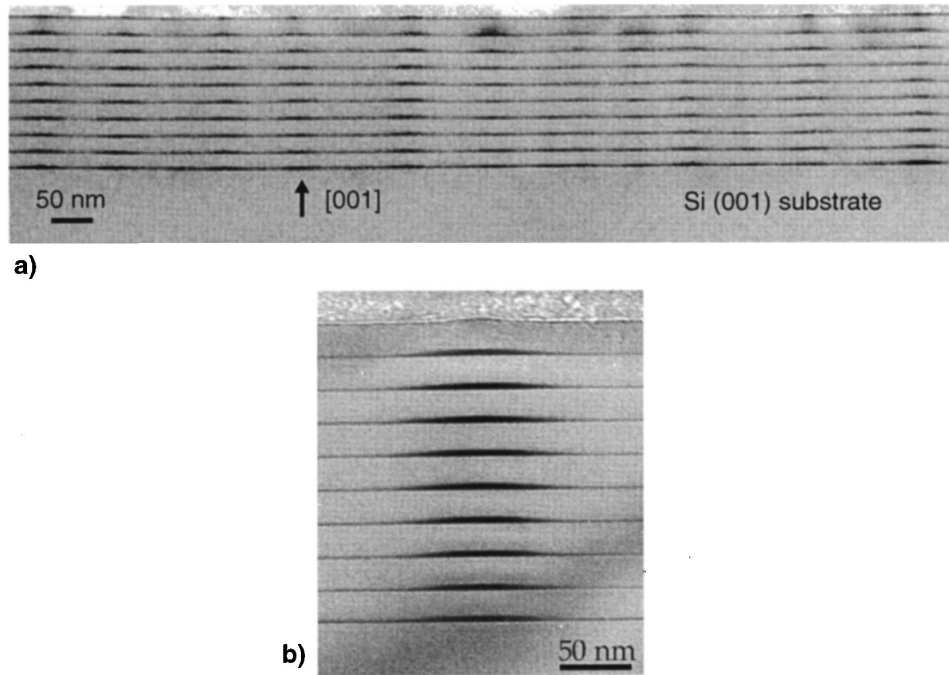


FIG. 6. (a) Typical cross-sectional TEM image taken along the  $[011]$  azimuth of a sample with 10 Ge/Si bilayers, the last Ge layer was not covered with Si. The deposited Ge amount was no longer kept constant but adjusted with the RHEED 2D-3D growth mode transition in each layer [see Fig. 5(b)]. (b) A zoom of an island column along the growth direction. It is important to note that the islands have almost equal size and height in all layers. The average island size is  $\sim 95$  nm and the average height is 6–7 nm.

average size of islands is  $\sim 80$  nm, their height is  $\sim 6$  nm. The island density is about  $2.5 \times 10^9 \text{ cm}^{-2}$ . What is more surprising is that the islands observed here are even smaller (in particular in height) than the islands on a single layer [Figs. 3(a) and 3(b)]. This clearly indicates that the island nucleation process has been significantly modified due to the presence of elastic strain induced by buried layers. Another interesting feature observed in this image is that the islands are arranged in an almost perfect hexagonal symmetry, resulting in a very regular interisland spacing. Indeed, only in a hexagonal symmetry the interisland spacing can be equivalent along all crystallographic directions. This result suggests that the surface diffusion of adatoms and/or islands is the dominant mechanism which governs the lateral ordering of islands in multilayer structures.

The low-temperature photoluminescence of the corresponding sample is shown in Fig. 8(a). A spectacular result is that the PL component corresponding to the wetting layers has almost disappeared, a behavior recently observed but only on “precursor clusters” having much smaller dimensions (of  $\sim 45$  nm in size and  $\sim 1$ – $2$  nm in height).<sup>4</sup> We note that the weak peak observed at  $\sim 1034$  meV is due to the combination of transverse optical (TO) and zone center ( $O^T$ ) phonons of the silicon substrate.<sup>17</sup> The quenching of the wetting layer PL component can be explained by the fact that the carriers which were created in the Ge WL’s and the Si spacer layers have been efficiently transferred into the islands, suggesting a high probability of radiative recombination of such islands. It is interesting to note that the PL spectral shape of the islands grown in this condition differs from the island spectral shape reported in Fig. 4(b). The island-related component is now reduced to a single line (apparently the excitonic no-phonon transition) instead of NP and TO assisted

recombination lines. This feature clearly indicates the influence of the island dimension on the interband PL signature. Comparison of Figs. 4(a), 4(b), and 8(a) appears to show that islands with sizes smaller than  $\sim 100$ – $110$  nm exhibit their

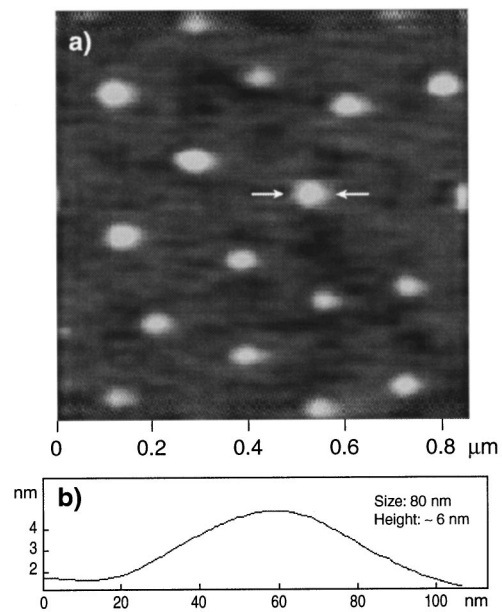


FIG. 7. (a) AFM image of a ten-bilayer sample in which the Ge deposited amount in each layer is adjusted with the 2D to 3D growth mode transition. The scan area is  $0.85 \mu\text{m} \times 0.85 \mu\text{m}$ . The islands have an average size of  $\sim 80$  nm and a height of  $\sim 6$  nm. Note that the islands are arranged in an almost perfect hexagonal symmetry, resulting in a very regular interisland spacing. (b) AFM height profile along the island indicated by two small arrows in (a).

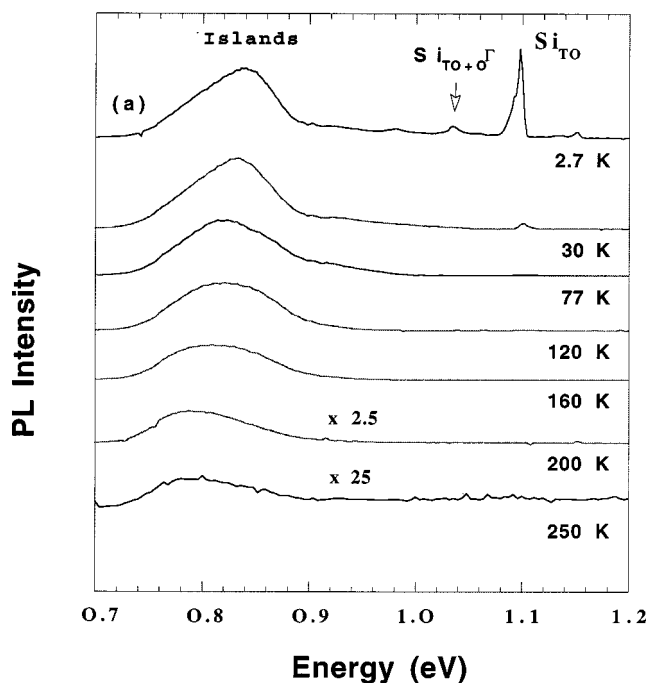


FIG. 8. PL temperature dependence of a ten-bilayer sample in which the Ge deposited amount in each layer is adjusted with the 2D to 3D growth mode transition. Note that in the 2.7 K spectrum, the wetting layer components have almost disappeared, indicating that the carriers being created in the Ge WL's and in the Si barrier layers have been efficiently transferred into the islands.

interband PL in a single line, while larger islands manifest themselves in a NP-TO pair. To further investigate the optical properties of such islands, we have measured the temperature dependence of the island PL (Fig. 8). The Si substrate component is quenched at  $\sim 30$  K while the island PL persists up to 250 K. The quenching of the island PL at high temperatures is attributed to the thermionic emission of the carriers from the Ge islands to the Si barrier. It is worth

noting that with increasing the temperature the island-related PL line exhibits a slight shift to lower energy, approaching the energy position of the islands in the single layer. Apart from a variation of the island bandgap with temperature, this shift can be partly explained by the fact that the multilayer sample consists of islands of different sizes in subsequent layers, resulting in different confinement potential. Due to strain-driven nucleation, islands in the upper layers may have sizes smaller than those on the single layer. Since islands of larger sizes have a deeper confinement potential, when the temperature increases the thermionic emission of the carriers toward the Si barriers will first occur for the less deep levels, i.e., for small islands in the upper layers. The PL of the larger islands on the first layer, in which the carriers are more deeply confined, is maintained at higher temperatures.

In conclusion, we have given evidence both from structural and optical characterizations, that the decrease of the Ge wetting layer thicknesses in the upper layers is the main mechanism which leads to the increase of the island sizes and heights in multilayer Ge/Si structures. Such a decrease of the Ge wetting layer thickness can be explained by an accumulation of homogeneous elastic strain induced by the buried Ge wetting layer(s). Though much effort still remains to be done to understand in a more quantitative manner the evolution of the islands as well as of the wetting layer in each layer, it is believed that the present finding opens, on one hand, the ways to produce Ge islands having equal size in all layers, and introduces, on the other hand, a new physical parameter in the growth process of a multilayer structure.

The authors would like to thank D. Débarre for his assistance during AFM measurements and A. Charrier for her constant help in graphic and photographic work. This work was partially supported by CNET under Convention, No. 981B044. One of us (V.L.T.) would like to thank the MENRT-CNRS for financial support for his project on the Ge/Si nanostructures (Grant No. PC/LK 98.375) in the framework of "Actions Spécifiques MENRT-DS2."

\*Author to whom correspondence should be addressed. Electronic address lethanh@ief.u-psud.fr

<sup>1</sup>See, for example, G. Abstreiter, P. Schittenhelm, C. Engel, E. Silveira, A. Zrenner, D. Meertens, and W. Jäger, *Semicond. Sci. Technol.* **11**, 1521 (1996).

<sup>2</sup>P. Boucaud, V. Le Thanh, S. Sauvage, D. Débarre, and D. Bouchier, *Appl. Phys. Lett.* **74**, 401 (1999).

<sup>3</sup>D. J. Eaglesham and M. Cerullo, *Phys. Rev. Lett.* **64**, 1943 (1990).

<sup>4</sup>V. Le Thanh, P. Boucaud, D. Débarre, Y. Zheng, D. Bouchier, and J.-M. Lourtioz, *Phys. Rev. B* **58**, 13 115 (1998).

<sup>5</sup>J. Tersoff, C. Teichert, and M. G. Lagally, *Phys. Rev. Lett.* **76**, 1675 (1996).

<sup>6</sup>C. Teichert, M. G. Lagally, L. J. Peticolas, J. C. Bean, and J. Tersoff, *Phys. Rev. B* **53**, 16 334 (1996).

<sup>7</sup>Q. Xie, A. Madhukar, P. Chen, and N. P. Kobayashi, *Phys. Rev. Lett.* **75**, 2542 (1995).

<sup>8</sup>A. A. Darhuber, V. Holy, J. Stangl, G. Bauer, A. Krost, F. Heinrichsdoff, M. Grundmann, D. Bimberg, V. M. Ustinov, P.

S. Kop'ev, A. O. Kosogov, and P. Werner, *Appl. Phys. Lett.* **70**, 955 (1997).

<sup>9</sup>L. Vescan, W. Jäger, C. Dieker, K. Schmidt, A. Hartmann, and H. Lüth, *Mater. Res. Soc. Symp. Proc.* **263**, 23 (1992).

<sup>10</sup>P. Schittenhelm, G. Abstreiter, A. Darhuber, G. Bauer, P. Werner, and A. Kosogov, *Thin Solid Films* **294**, 291 (1997).

<sup>11</sup>P. Schittenhelm, C. Engel, F. Findeis, G. Abstreiter, A. Darhuber, G. Bauer, A. O. Kosogov, and P. Werner, *J. Vac. Sci. Technol. B* **16**, 1575 (1998).

<sup>12</sup>E. Mateeva, P. Sutter, J. C. Bean, and M. G. Lagally, *Appl. Phys. Lett.* **71**, 3233 (1997).

<sup>13</sup>M. Goryll, L. Vescan, and H. Lüth, *Thin Solid Films* **336**, 244 (1998).

<sup>14</sup>V. Le Thanh, D. Bouchier, and D. Débarre, *Phys. Rev. B* **56**, 10 505 (1997).

<sup>15</sup>J. Weber and M. I. Alonso, *Phys. Rev. B* **40**, 5683 (1989).

<sup>16</sup>V. Le Thanh, *Thin Solid Films* **321**, 98 (1998).

<sup>17</sup>P. J. Dean, J. R. Haynes, and W. F. Flood, *Phys. Rev. B* **161**, 711 (1967).